The EUMETSAT Network of Satellite Application Facilities

GRAS SAF
GRAS Meteorology

GRAS SAF CDOP Visiting Scientist
VS7

Collocating GRAS with nadir sounders onboard of Metop: An assessment for instrument and climate monitoring

Florian Ladstädter

March 6, 2012

Version 1.1
SAF/GRAS/DMI/REP/VS07/001

Contents

List of Figures

List of Tables

Abstract

The Metop satellite hosts several instruments that are sensitive to the atmospheric temperature profile, e.g., AMSU-A, HIRS, IASI, and GRAS. The nadir sounders AMSU-A, HIRS, IASI are collocated, but GRAS observes in limb sounding view either ahead of the satellite (rising occultations) or behind the satellite (setting). Most of the occultations are actually on the nadir swath, but with a few minutes ahead or delayed. The hosting of a radio occultation instrument along with nadir sounders opens an opportunity to use these continuous collocations for instrument monitoring. In particular collocations of the AMSU-A with GRAS are promising since AMSU (and previously MSU) are instruments used to generate long term data sets for climate monitoring. AMSU-A channel 9—one of the channels primarily used for these long term data sets—is peaking in the lower stratosphere, thus the use of GRAS radio occultation measurements can be restricted in this case to altitudes where no ambiguity of water vapor and temperature is present. Investigating other instruments/other channels/water vapor can be performed at a later stage. The work will also allow a first assessment on whether radio occultation can contribute to GSICS and thus responds to a recommendation expressed at the first workshop of the International Radio Occultation Working Group (IROWG).

1 Introduction

Satellite observations of upper-air temperature have been dominated by the Microwave Sounding Unit (MSU) and the Advanced MSU (AMSU) instrument for the last several decades. These instruments flying on National Oceanic and Atmospheric Administration (NOAA) polar orbiting satellites were the only source for long-term temperature measurements of global coverage. The calibration of time series containing data from only one source is inevitably a demanding task (Thorne et al. 2005; Christy et al. 2006). This poses challenges on climate studies, where trend signals can easily be masked by spurious time-varying biases. Due to these restrictions, knowledge about upper-air temperature trends is still limited (Trenberth et al. 2007; Santer et al. 2008; Thorne et al. 2011). Furthermore, the bias corrections needed when assimilating AMSU data in Numerical Weather Prediction (NWP) models can also be substantial.

It is therefore obvious that new, independent datasets to reduce the structural uncertainties involved are needed. The importance of reference observations to calibrate observations has been stated by different institutions (Karl et al. 2006; GCOS 2010). The implementation plan for Global Observing System for Climate (GCOS) lists requirements for records of climate quality. According to these guidelines, a long-term record involving a series of instruments requires a suitable period of overlaps to assure sufficient calibration and monitoring. They also include the need for reference observations.

In this context, the series of Meteorological Operational (Metop) satellites provides unique opportunities to both meteorological and climatological applications. The Metop satellites aim to “to provide continuous, long-term data sets, in support of operational

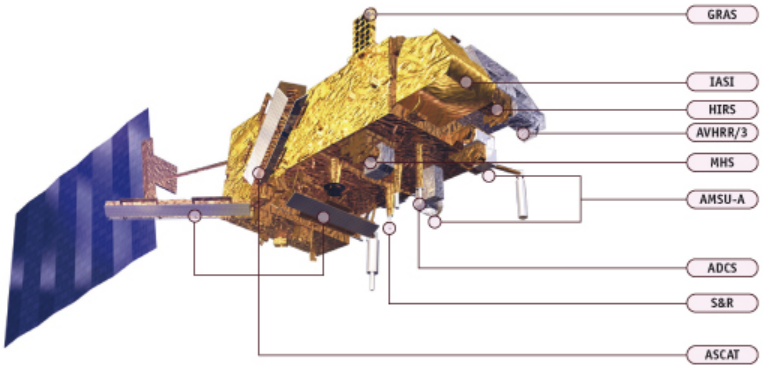

Figure 1: Instruments on Metop. Image by EUMETSAT.

meteorological and environmental forecasting and global climate monitoring".[1] They are part of the European Organisation for the Exploitation of Meteorological Satellites (EUMETSAT) Polar System (EPS), consisting of three satellites flown successively for at least 16 years. EUMETSAT follows the GCOS principles by including sufficient overlap periods for these three satellites.

The first of them, Metop-A, has been in orbit since October 2006. Metop carries both state-of-the-art instruments such as GNSS Receiver for Atmospheric Sounding (GRAS) or Infrared Atmospheric Sounding Interferometer (IASI), and instruments which have been in use for a longer time period within the NOAA satellite program, such as AMSU or High resolution Infrared Radiation Sounder (HIRS) (Figure 1).

The inherent low systematic error of the RO technique employed by the GRAS instrument makes it a candidate for providing potential reference measurements (Leroy et al. 2006; Leroy et al. 2008; Steiner et al. 2009; Ho et al. 2009a). Observing from the same platform gives a high number of collocated measurements from the different types of instruments, and avoids uncertainties stemming from different sampling characteristics. In this initial study, the opportunity of having the GRAS RO instrument alongside AMSU shall be used to assess the prospect of inter-calibration and instrument monitoring using GRAS (see also Engeln et al. 2011). This can potentially also improve the contribution of AMSU to weather forecasting and climate monitoring.

1.1 MetOp

EUMETSAT Polar System (EPS) Metop mission series is Europe's first series of polar-orbiting satellites. It consists of three successive Low Earth Orbit (LEO) satellites with an overlap time of about half a year, providing operational services until around 2020. The Metop satellites fly in a sun-synchronous orbit (equator crossing Local Solar Time (LST) at 9:30 in descending node) at an altitude of about 820 km and an inclination of 98.70° (Klaes et al. 2007). The completion of one orbit takes about 100 min.

[1] www.eumetsat.int/Home/Main/Satellites/Metop/MissionOverview

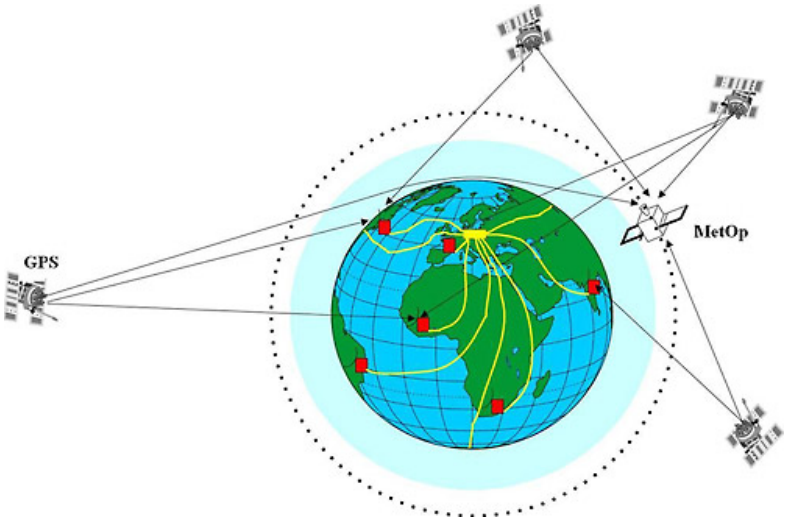

Figure 2: GRAS measurement principle. Image by EUMETSAT, GRAS product guide.

Several of the instruments on board of Metop are able to give information about atmospheric temperatures: IASI, AMSU, HIRS, and GRAS. While the first three of these instruments are observing in nadir geometry, and are therefore collocated, the GRAS instrument uses the RO method to observe in limb view. The RO instrument observes the horizon, and measurements of corresponding areas of the atmosphere occur typically a few minutes ahead or delayed compared to the nadir sounders. To be used for comparisons, the RO occultations must first be matched to corresponding nadir measurements using sensible collocation criteria.

1.2 GRAS

One of the instruments on board of Metop is GRAS, an RO instrument observing rising and setting occultations from Global Positioning System (GPS) satellites (Figure 2).

The RO technique uses electromagnetic signals transmitted by GPS satellites, which are delayed and refracted by the atmosphere. The basic quantity measured are phase changes of these signals. These phase changes are converted into profiles of bending angles α. The bending angles are the integrated incremental bending along the ray path. Applying an Abel transform inverts these angles to profiles of refractivity N. Since bending angles are characterized by large noise at high altitudes (upper stratosphere and higher), this integration would lead to non-negligible errors in the refractivity profiles. Therefore the bending angle profiles are initialized using background information at high altitudes. It is then "optimized" in a statistical optimal way to yield an improved combined bending angle profile. There is a trade-off between the amount of background data introduced using statistical optimization and the improved quality of refractivity profiles.

The refractivity is related to other atmospheric parameters of interest by the Smith-

Weintraub relation, which in its simplified form states:

$$N = 77.6\frac{p}{T} + 3.73 \times 10^5 \frac{e}{T^2},$$

where p is the atmospheric pressure (hPa), T the temperature (K), and e the partial pressure of water vapor (hPa). In the stratosphere and upper troposphere, where moist content is low, the second (moist) term can be neglected, leaving a remaining dry term, directly proportional to air density ρ. Density is transformed to pressure via the hydrostatic equation, and then to temperature using the ideal gas law. The underlying assumption of dry air conditions means that the retrieved parameters T_{dry} and p_{dry} are strictly speaking no physical parameters, although the difference to physical temperature and pressure can be small. In the lower troposphere, water vapor effects dominate refractivity. In this region, temperature and water vapor profiles can be retrieved using background information and 1D variational data assimilation schemes. The retrieved temperature reflects physical temperature in this case, but the ratio of background to observational information contained needs to be carefully evaluated.

The GRAS receiver on board of Metop is able to track more than 600 occultation soundings per day. GRAS has a nominal sampling rate of 50 Hz. It is also capable of tracking in "raw sampling" mode (also called "open loop" mode) at 1 kHz, and this mode is used for the lowest part of the atmosphere (Luntama et al. 2008).

The horizontal resolution of RO is limited by the limb sounding approach and is approximately 100 km to 300 km, whereas the vertical resolution can be as good as 100 m.

1.3 AMSU

The AMSU-A instrument on board of Metop is provided by NOAA and brings continuity to previous and ongoing NOAA Polar Operational Environmental Satellite (POES) missions (NOAA-15, -16, -17, -18). AMSU was introduced in 1998 as an upgraded version of the original MSU instrument. The first MSU instrument started continuous observations already in late 1978 as part of the Television Infrared Observation Satellite (TIROS) spacecraft.

AMSU-A measures layer-average brightness temperatures.[2] It is a 15-channel radiometer exploiting mainly microwave emissions of oxygen molecules (Spencer et al. 1990). The vertical resolution is coarse, and the delivered temperatures are single values describing a rather thick layer of the atmosphere. By choosing the channel (frequency), different height regions of the atmosphere are sampled, as shown by weighting functions describing the vertical contribution (Figure 3).

AMSU is a cross-track scanning radiometer. It scans from West to East for ascending passes with a scan range of ±48° with respect to nadir. This corresponds to a swath width of ±1026 km (Figure 4). Each scan samples 30 Earth views (pixels), two views of the internal warm target, and two views of cold space. It takes 8 sec to complete. The cold space and warm target views are used for calibration. The approximate zenith

[2]The brightness temperature is the temperature a black body with the same intensity as observed from the real gray body would have.

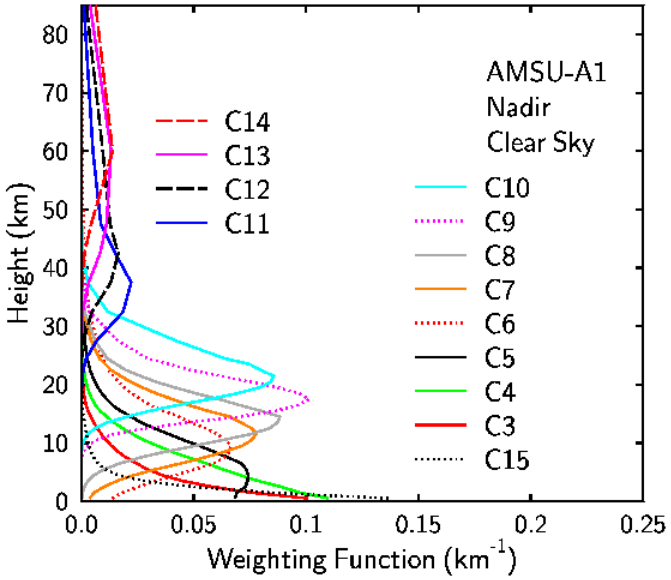

Figure 3: AMSU weighting functions, describing the contribution that microwave radiation emitted by a layer makes to the total intensity measured. Image taken from http://amsu.cira.colostate.edu/weights.html.

angles for the Earth view pixels from the edges to nadir are (in deg; symmetric with regard to nadir): 57.6, 53.0, 48.7, 44.5, 40.4, 36.4, 32.4, 28.5, 24.7, 20.8, 17.0, 13.2, 9.4, 5.6, 1.9.

The Instantaneous Field of View (IFOV) is approximately 3.3°. This leads to a nearly circular IFOV of 47.63 km at nadir and of 146.89 km (across track) and 78.79 km (along track) at the edges. The distance between two adjacent scanning lines is 52.69 km (*ATOVS Level 1b Product Guide* 2010).

2 Data and Method

For this initial study, data for the time period from October 1, 2007 to October 27, 2007 was chosen. The data were provided by GRAS Satellite Application Facility (GRAS SAF), EUMETSAT, and European Centre for Medium-Range Weather Forecasts (ECMWF).

2.1 RO

The GRAS RO data consist of dry temperature output of RO Processing Package (ROPP) (Offiler et al. 2011) as well as 1D-var physical temperatures using ECMWF forecasts as background (with the 1D-var assimilation working on refractivity level). The raw phase delay data—used as input to ROPP—were provided by EUMETSAT. For the initialization at high altitudes and statistical optimization at 40 km to 60 km,

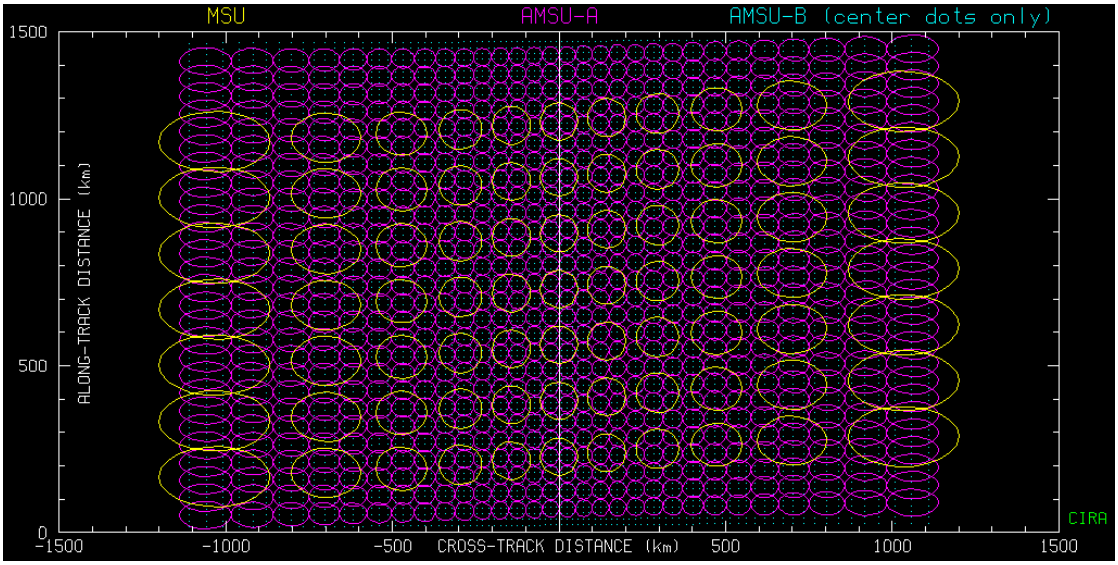

Figure 4: Earth-surface footprints for AMSU-A (purple), MSU (yellow) and AMSU-B (turquoise dots). The extensions of the 30 AMSU-A pixels on Earth from edge to edge (left to right) and along-track (bottom to top) are visible. Image taken from http://amsu.cira.colostate.edu/.

both Mass Spectrometer and Incoherent Scatter Radar (MSIS) climatologies as well as ECMWF analyses were used and will be presented separately.

ROPP adds two "quality scores" to its output profiles which can be used to identify and remove data of low quality. These scores were originally introduced in Gorbunov et al. (2006). The "L2 quality score" ($L2\_badness\_score$) measures the quality of the L2 signal using an empirical penalty function. The "statistical optimization quality score" ($IC\_badness\_score$) is based on error variances of the bending angle solution and measures both the quality of the match between the data and fitted profile used for the statistical optimization and the noise of the L1 signal. In this study, all profiles with $L2\_badness\_score > 30$ and $IC\_badness\_score > 25$ were rejected.

A first version of the study data showed an unexpected large spread in differences of collocated RO and AMSU data. This could be traced back to large noise in bending angles at high altitudes, caused by a subtle sign convention mismatch in the reconstruction of L2 phases. The comparison study helped revealing this problem in the RO data, demonstrating a first helpful outcome.

2.2 AMSU

The corresponding Metop AMSU level 1b data for October 2007 were provided by EUMETSAT. They consist of brightness temperatures for three AMSU channels (8, 9 and 10), together with metadata (time and geolocation, pixel number and corresponding zenith angle, and some quality flags). Only AMSU data with good quality as indicated

by the quality flags are used. Data where the angle between space view and moon is below 4° are skipped because of possible calibration issues there (this restriction applies to no data points within the considered time frame though).

2.3 ECMWF

ECMWF data are used in this study at various occasions: Collocated ECMWF analyses profiles are used as an additional dataset to compare with; humidity and surface values from these analyses files are used to provide the radiative transfer model (subsection 2.4) with its required additional input; ECMWF analyses are used for the statistical optimization in one study case (subsection 2.1); and ECMWF forecast files are used for the 1D variational scheme to arrive at physical temperatures. To collocate the ECMWF data to the RO occultations, the four nearest grid points are interpolated bilinearly to the occultation point, using the closest of the four analyses time layers (0 UTC, 6 UTC, 12 UTC, and 18 UTC).

2.4 Setup of comparable data

The comparison of collocated data in this study is based on AMSU-equivalent brightness temperatures for three different upper-tropospheric/stratospheric channels. To compute synthetic layer-average brightness temperatures from RO and ECMWF profiles, the Radiative Transfer for TOVS (RTTOV) model in version RTTOV v10 is used (Saunders 2011a). RTTOV allows simulations of radiances (brightness temperatures) for satellite nadir radiometers given a profile of temperature, water vapor, and surface parameters (Saunders 2011b). Water vapor and surface parameters are taken from collocated ECMWF profiles (except for 1D-var data, where water vapor is included). This is justified because neither surface parameters nor water vapor have any significant influence on the resulting top layer brightness temperatures for the altitude regions under consideration in this study.[3]

The three AMSU channels used are 8, 9, and 10 (see Figure 3 for corresponding height ranges). For each collocated RO/AMSU pair, the equivalent brightness temperatures for these three channels are calculated considering also the zenith angle for the respective AMSU pixel. The zenith angle is specified as an additional input parameter to RTTOV and effectively changes the height of the weighting function peaks.

2.5 Collocations and geometry

Metop enables observations by different instruments mounted on the same platform. This inherently leads to a high number of collocated measurements. Comparing such collocated data avoids uncertainties usually stemming from different sampling characteristics. In the case of comparing passive nadir sounders such as AMSU with active instruments observing the horizon such as GRAS, locally collocated measurements will

[3]Changing the humidity profile provided to RTTOV by, e.g., exchanging ECMWF analysis and forecast humidity profiles has no effect on the resulting brightness temperatures (not shown).

Table 1: Number of matched AMSU pixels and RO profiles for two collocation criteria; number of AMSU pixels collocated on average to one RO profile.

Criteria	Matched AMSU (of 8684520)	Matched RO (of 17873)	AMSU pixels per RO profile
≤50 km, ≤30 min	13663 (0.16 %)	6372 (35.65 %)	2.1
≤300 km, ≤180 min	1255188 (14.45 %)	16472 (92.16 %)	76.2

have a time offset. Due to the occultation geometry, a collocation is not everywhere possible and the number of collocations furthermore has a dependency on latitude.

Given Earth's radius of around 6367 km and an altitude for Metop of around 820 km, RO observes the local horizon at a distance of approximately 3300 km. Together with the AMSU swath width of around 1000 km from the satellite track, this results in all collocations occurring closer than approximately 20° to the satellite track (forward and backward looking), as long as the collocation criteria restrict possible collocations to the same orbit. For larger criteria, also collocations between two adjacent orbits are possible.

As shown by Santerre (1989), even the full GPS constellation does not provide a uniform distribution of visible satellites in the sky. As a result of the inclination of GPS satellite orbits, the satellite sky distribution is a function of the observer's latitude.

This has interesting consequences especially around the equator: In Figure 5 the area of the observer's sky where it is not possible to make observations is shown on polar plots (azimuth vs. zenith angles) for different observer's latitudes. For the equator ($\phi = 0°$), no observations of GPS satellites are possible at the horizon within about 30° from north or south.

This shadow area leads to a gap in collocations near the equator, because at an Metop inclination angle of 98.70° and for all collocations occurring closer than 20° to the satellite track, there will never be any setting or rising GPS satellite observed there. The gap disappears when the collocation criteria are chosen such that collocations between different orbits are possible (Figure 6).

For the time period under consideration in this study, data from a total number of 17873 RO profiles and 8684520 AMSU pixels were available. The number of matches for two collocation criteria are summarized in Table 1. To determine the distance between RO profiles and AMSU pixels, the location of the RO tangent point at the approximate height of the corresponding weighting function peak is used. Due to the limited horizontal resolution of RO soundings, this location can only be an approximation. This limits the accuracy of collocations and introduces a possible source of collocation errors.

For the "small" criterion allowing matches only within 30 min (same orbit only), around 36 % of all RO profiles have collocated AMSU data. For the "large" criteria (adjacent orbits also within reach), more than 92 % of RO profiles are matched.

Figure 7 shows the spatial extend of these collocation criteria over Europe, together with (for the "small" criteria) all collocations within the study time period and (for the

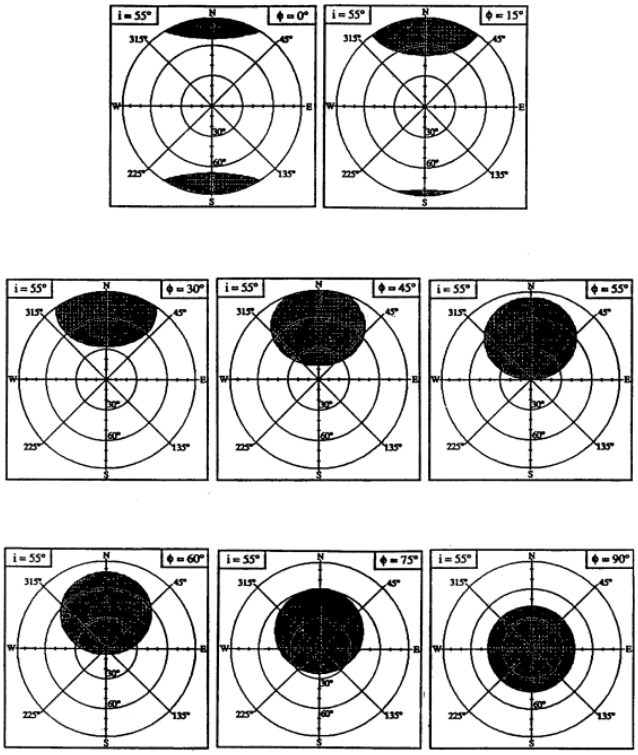

Figure 5: Shadow areas where GPS satellites cannot be observed as a function of site latitude (for a GPS satellite orbital inclination of 55 deg). Taken from Santerre (1989, p. 14).

"large" criteria) all collocations on one day with indication to which orbit they belong.

The constraints on collocation geometry lead to rather sharp peaks in the distribution of time differences between collocated RO and AMSU observations (Figure 8). All collocations in the same orbit occur approximately within ±8 min (rising and setting occultations; the small change in time difference between rising and setting results from the duration of one occultation). Collocations including the adjacent orbits occur approximately within ±100 min, related to the orbit period.

3 Results

All results in this section are using robust statistics (bisquare weighting) to make mean and standard deviation calculations less sensitive to outliers from the distribution. Collocation criteria are ≤50 km, ≤30 min, if not indicated otherwise.

3.1 Detecting biases

A number of studies have shown that RO measurements are essentially bias-free and of high accuracy (e.g., Ho et al. 2009b; Scherllin-Pirscher et al. 2011), especially in the height region of interest in this study. Accurate and stable observations are crucial for

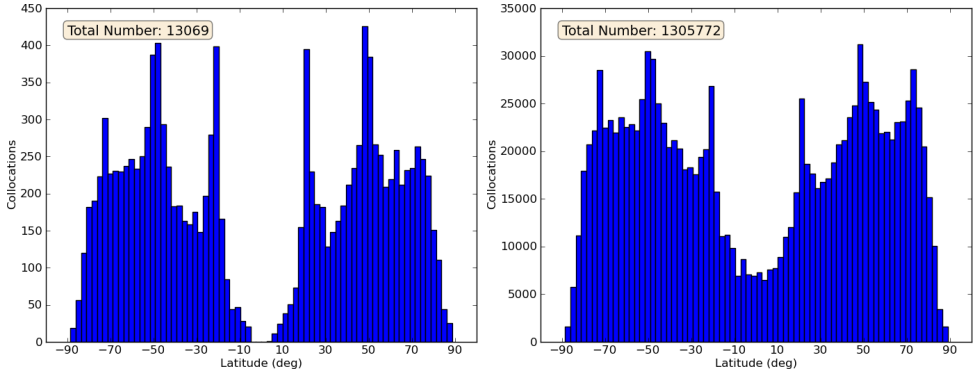

Figure 6: Number of RO/AMSU matches by latitude (2.5° bin size). Collocation criteria are: (left) ≤50 km, ≤30 min; (right) ≤300 km, ≤180 min.

climate change detection and high-quality NWP applications. The properties of RO make this technique useful to assess the quality of other instruments such as AMSU. AMSU requires time-varying bias-corrections before being assimilated into NWP or being used for long-term climate records. Collocated RO observations can potentially be used to constantly monitor and bias-correct AMSU.

In Figure 9 (left) the differences between collocated RO and AMSU brightness temperatures are shown for three channels. The overall biases here are latitude-independent to some extend: For channel 8, the distribution shows an overall bias of 1.0 K, for channel 9 no bias, and for channel 10 a bias of −0.25 K.

3.2 RO noise: Statistical optimization

It is noticeable that the standard deviation of the difference distribution in Figure 9 (left) increases by about a factor of two when going from the lowest channel 8 to channel 10. The differences between ECMWF and AMSU (Figure 9 (right)) do not show this behavior. This indicates that the larger spread for channels higher up stem from increasing RO data noise, and is most probably an effect of the statistical optimization needed to initialize RO profiles at high altitudes (subsection 1.2).

In Figure 9 (left) the MSIS climatology is used for the bending angle initialization by searching for the best fitting MSIS profile. As a test for the assumption that the statistical optimization causes the increase in standard deviation, the same comparison with AMSU was performed but using collocated ECMWF analyses for the initialization step (Figure 10).

Using ECMWF analyses with their high spatial and temporal resolution has the presumed effect that the increase in spread when going to higher channels becomes less pronounced. It is not disappearing, indicating that statistical optimization might still be an issue, especially for the highest channel 10. The number of outliers—notably emerging at high latitudes—is also decreasing when using ECMWF. It has to be noted though that using collocated ECMWF profiles instead of a generic MSIS climatology for “optimizing” bending angles, ECMWF background information is introduced in the

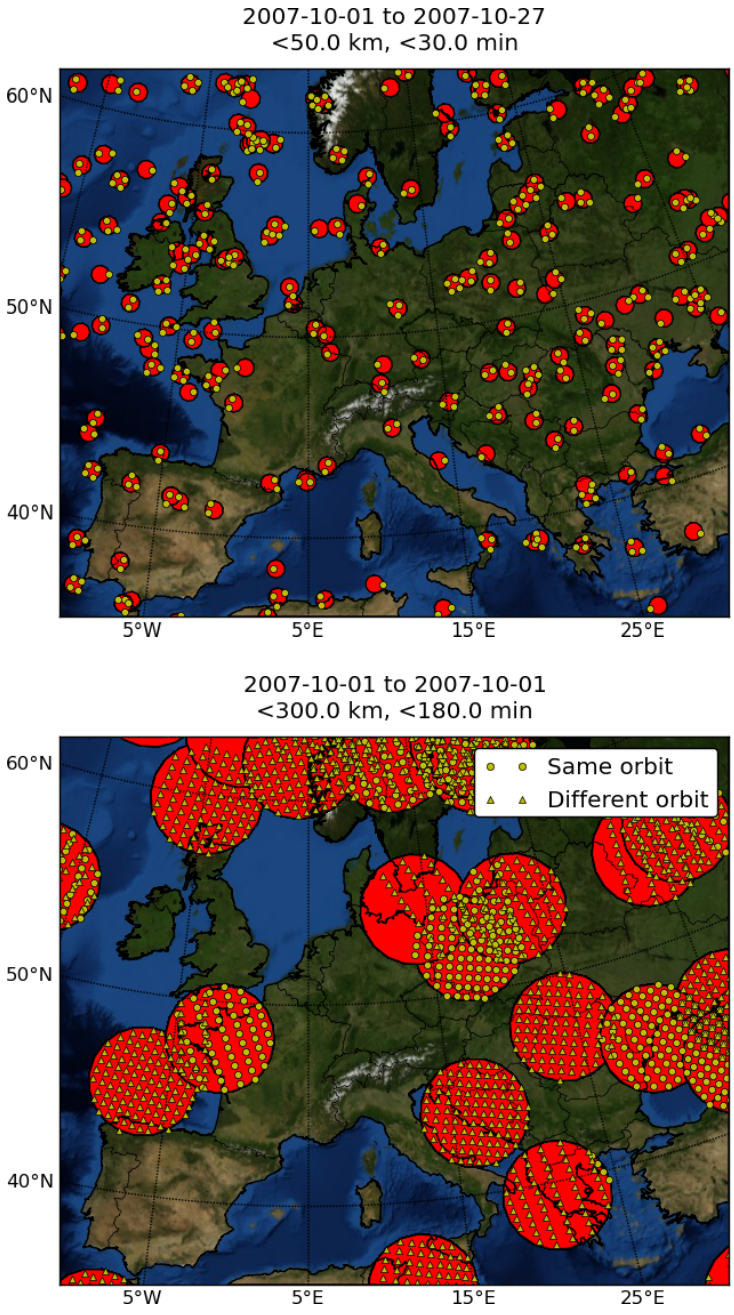

Figure 7: Collocations over Europe for (top) the whole study time period for the criteria $\leq$50 km, $\leq$30 min; and (bottom) for one day for the criteria $\leq$300 km, $\leq$180 min, indicating if the collocated AMSU pixel stems from the same or from an adjacent orbit. The centers of the red circles indicate the positions of the RO occultations, the yellow circles and triangles the position of the collocated AMSU pixels.

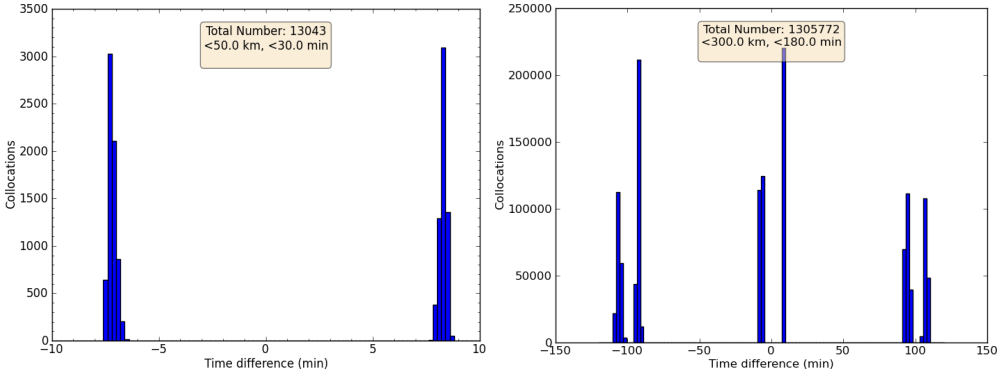

Figure 8: Time difference distribution of collocations for (left) ≤50 km, ≤30 min; (right) ≤300 km, ≤180 min.

retrieved RO profiles.

Figure 11 shows that the noisier bending angle profile above 40 km for MSIS initialization compared to ECMWF initialization translates into notable differences for the RO temperature profile also below 40 km. This has an impact on the integrated brightness temperatures especially for channel 10, with its weighting function peak above 20 km (Figure 3).

3.3 RO: Dry temperatures versus 1D-var

Only dry RO temperatures have been used so far. In Figure 12 physical temperatures from RO calculated with 1D-var assimilation using ECMWF forecasts as background data are compared to collocated AMSU and ECMWF analyses background data for channel 9. The standard deviation decreases by more than a factor of two for the difference of 1D-var temperatures versus AMSU compared to dry temperatures versus AMSU. The bias increases from around 0.0 K in the case of dry temperatures to −0.2 K for 1D-var temperatures, whereas it vanishes when comparing 1D-var temperatures to ECMWF analyses data.

Comparing 1D-var temperatures to ECMWF analyses data shows not only very small biases but also a substantial decrease in the standard deviation. This agreement is expected due to the large impact of RO data on the ECMWF analysis in this height interval. Future collocation studies could assess this impact and the amount of background data contained in the RO 1D-Var temperature, e.g. by comparing both ECMWF analyses and forecasts to RO and AMSU data.

Conversely, the remarkably small standard deviation of the difference between AMSU and ECMWF data might be due to the impact of AMSU satellite data on the ECMWF models (Cardinali 2009)—this should be subject of future work.

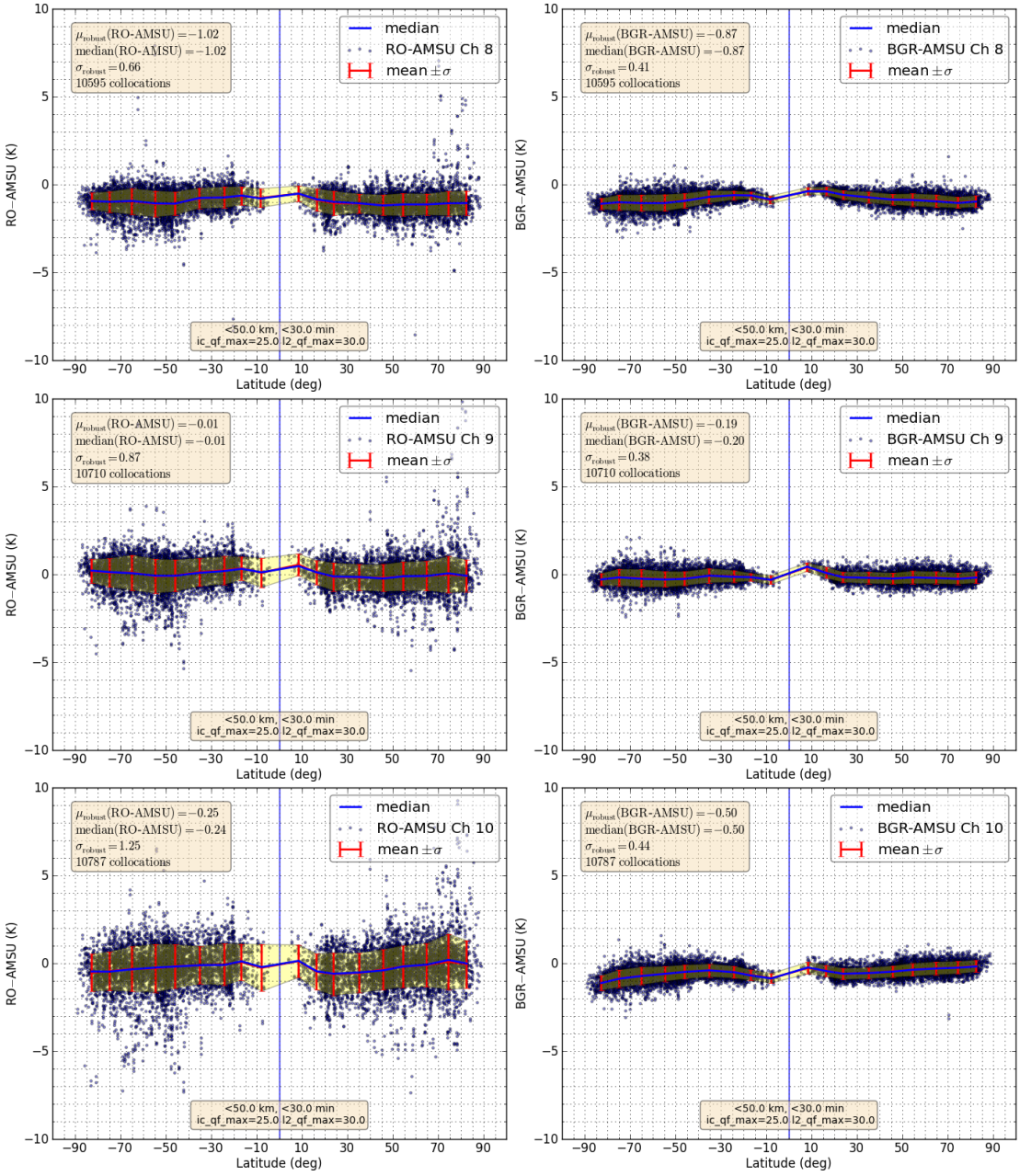

Figure 9: Differences of collocated RO–AMSU (left) and ECMWF–AMSU (right) brightness temperatures for channel 8 (top), 9 (center), and 10 (bottom). Median, mean and standard deviation are shown in 10° bins and for the whole distribution.

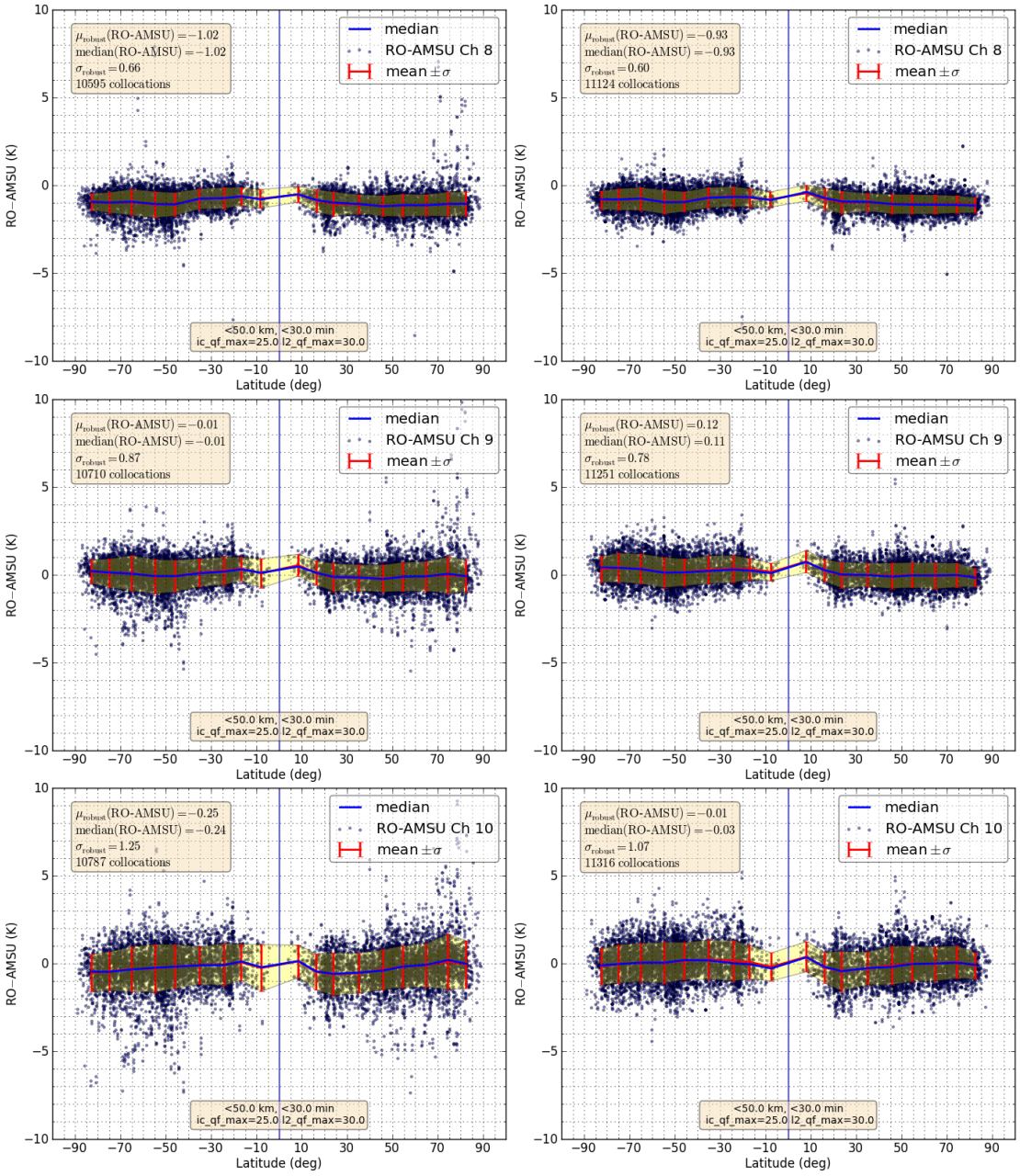

Figure 10: Differences of collocated RO–AMSU brightness temperatures for channel 8 (top), 9 (center), and 10 (bottom). Bending angles are initialized using MSIS climatology (left) and collocated ECMWF analyses (right). Median, mean and standard deviation are shown in 10° bins and for the whole distribution.

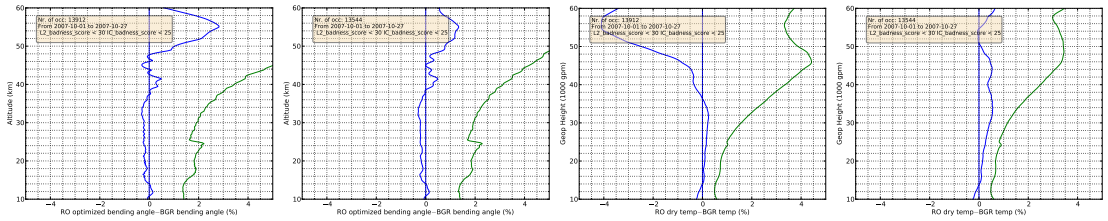

(a) MSIS (b) ECMWF (c) MSIS (d) ECMWF

Figure 11: Observation versus background (ECMWF) statistics for statistical optimization using MSIS climatology and ECMWF analyses. Optimized bending angles compared to background bending angles shown in (a) and (b); RO dry temperatures compared to background temperatures show in (c) and (d). Bias in blue, standard deviation in green.

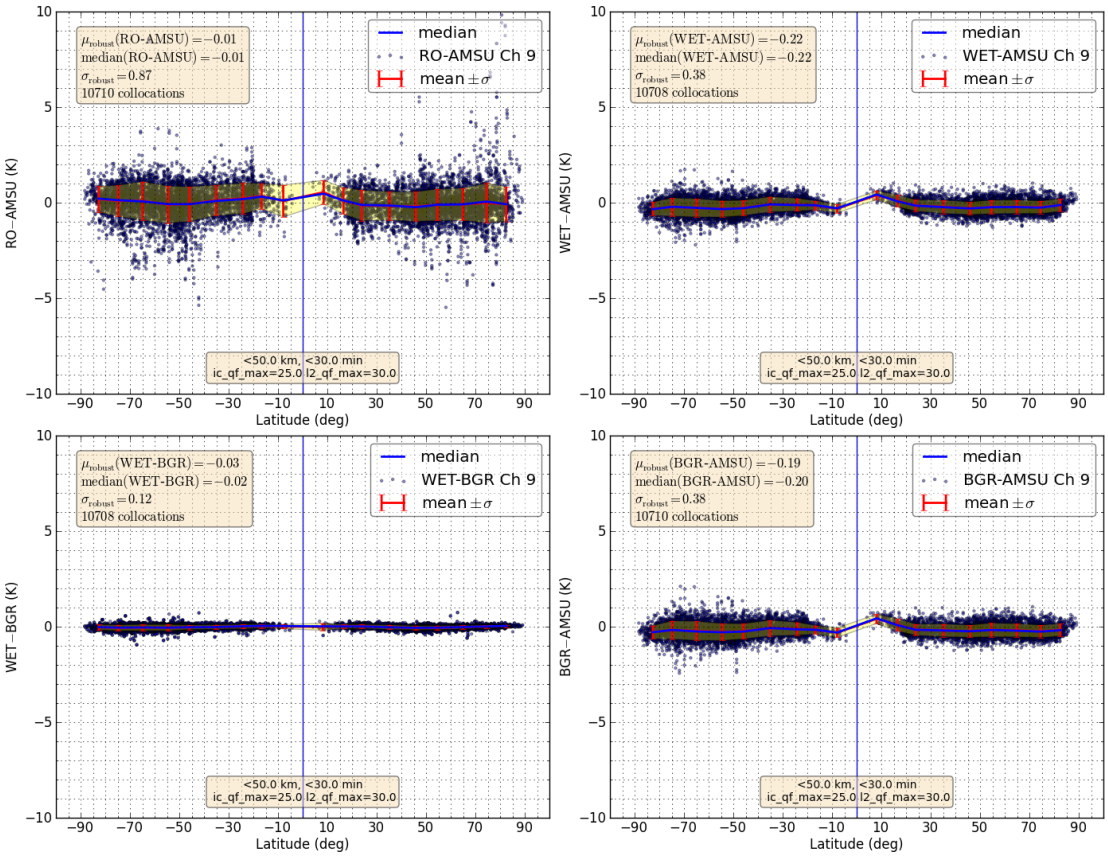

Figure 12: Differences of collocated RO–AMSU (top left), RO 1D-var–AMSU (top right), RO 1D-var–ECMWF (bottom left), and ECMWF–AMSU (bottom right) brightness temperatures for channel 9. Median, mean and standard deviation are shown in 10° bins and for the whole distribution.

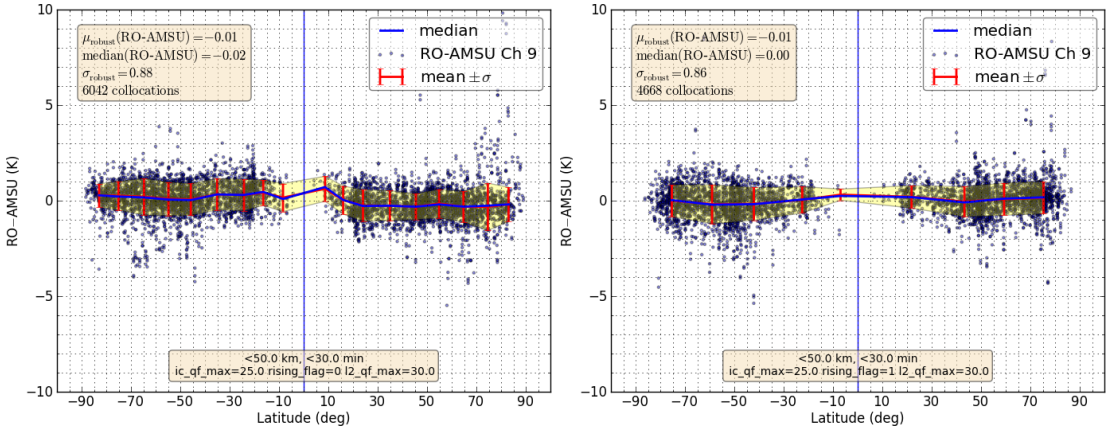

Figure 13: Differences of collocated RO–AMSU brightness temperatures for channel 9. Only setting (left)/rising (right) occultations are included. Median, mean and standard deviation are shown in 10° (left)/20° (right) bins and for the whole distribution.

3.4 RO: Rising and setting

To determine whether or not occultations occurring while looking backward (setting) or forward (rising) have differing characteristics, both types are plotted separately in Figure 13. Differences between setting and rising occultations are negligible.

3.5 Collocation criteria

Since the number of matches is already high when restricting collocations to the same orbit, it is optional to use the "large" collocation criteria as well. Figure 14 shows that there is not much additional information contained in comparison to the "small" criteria: The bias determined stays the same for all three channels, and although there is a lot of visual noise due to the huge number of collocations, the actual distribution does not change much. This indicates that the atmospheric variability is small also within $\leq$300 km, $\leq$180 min.

For the "small" criteria, each RO observation is matched to two AMSU pixels on average (Table 1). When restricting the collocations to the closest one only, the difference distribution is not changing (Figure 15).

3.6 Inspecting AMSU

The bias of AMSU observations changes when going from nadir to the swath edges. Using tightly collocated RO measurements can be a way to monitor the bias of AMSU measurements for different pixels. When limiting the maximum zenith angle to ±15° (Figure 16), the standard deviation remains largely unaffected, but there appears a consistent bias of around 0.2 K for all three channels in comparison to the unrestricted case.

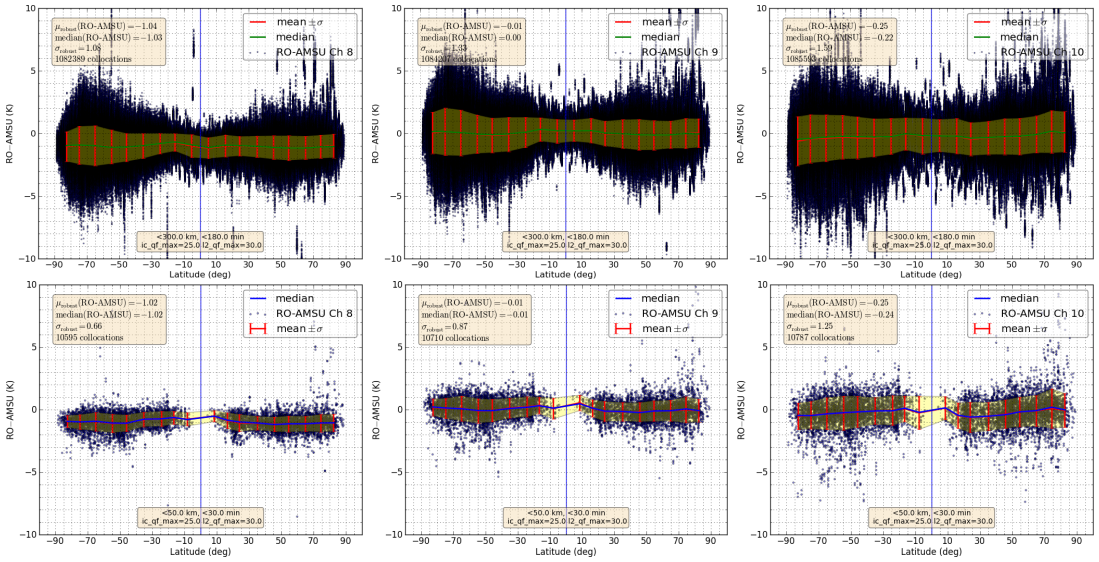

Figure 14: Differences of collocated RO–AMSU brightness temperatures for channel 8 (left), 9 (center), and 10 (right). Collocation criteria are $\leq$300 km, $\leq$180 min (top) and $\leq$50 km, $\leq$30 min (bottom). Median, mean and standard deviation are shown in 10° bins and for the whole distribution.

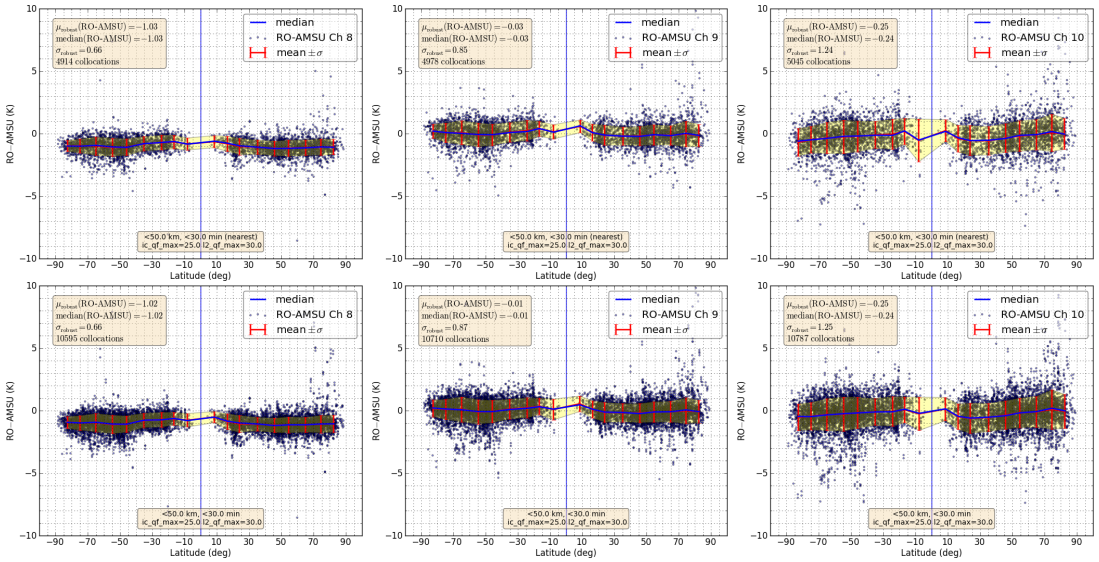

Figure 15: Differences of collocated RO–AMSU brightness temperatures for channel 8 (left), 9 (center), and 10 (right). In case of several AMSU pixels per RO observation, only the closest is taken (top) or all are shown (bottom). Median, mean and standard deviation are shown in 10° bins and for the whole distribution.

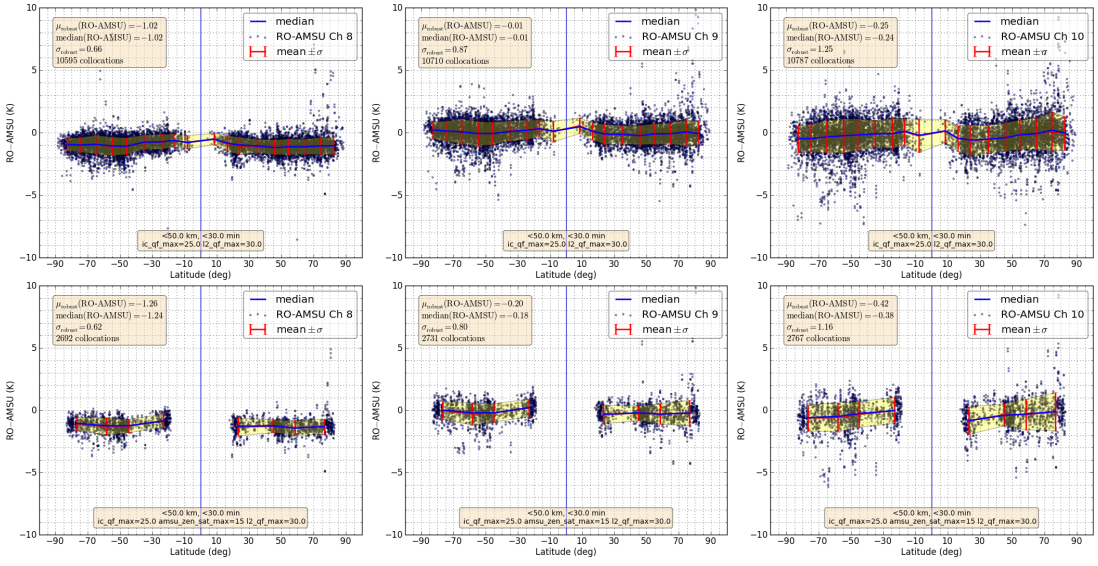

Figure 16: Differences of collocated RO–AMSU brightness temperatures for channel 8 (left), 9 (center), and 10 (right). No restriction on AMSU zenith angle (top), restricting AMSU scan zenith angle to ±15° (bottom). Median, mean and standard deviation are shown in 10° (top)/20° (bottom) bins and for the whole distribution.

AMSU has a scan range of ±57.6° (zenith angle; see subsection 1.3). A possible asymmetry in scanning in one versus the other direction (with regard to nadir) is examined in Figure 17. A bias of approximately 0.2 K between both scanning directions appears for all three channels.

4 Conclusions

GPS Radio Occultation measurements from the GRAS instrument on board of Metop were collocated and compared to AMSU measurements from the same platform. Observing from the same platform leads to a large number of collocations already for rather strict temporal and spatial matching criteria. Out of 17873 RO occultations for the test month, more than 35 % were matched with AMSU observations coming from the same orbit. When also including adjacent orbits, more than 90 % were matched. This shows the great potential of collocating nadir sounders with RO occultations from Metop.

The inherent absolute RO accuracy can be used to monitor and, eventually, calibrate nadir temperature sounders such as AMSU with RO. However, the choice of initializing and "optimizing" RO bending angles at high altitudes has to be considered carefully. The study showed a substantial influence of this choice especially for the investigated lower stratospheric channels 9 and 10. In this respect, this study was also valuable to evaluate processing choices for RO data.

The results of this work point to possible future directions of research:

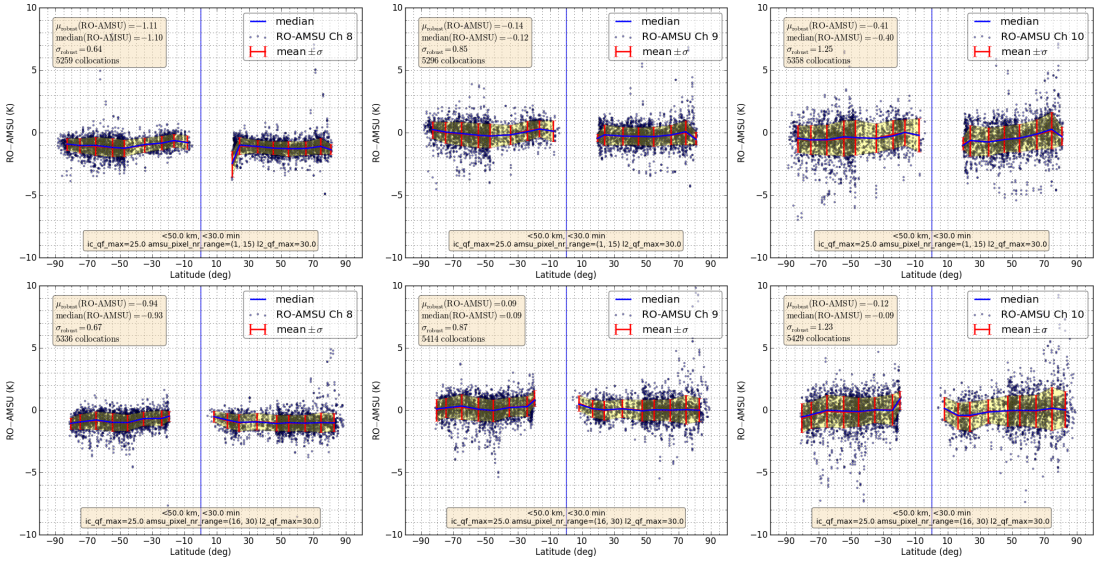

Figure 17: Differences of collocated RO–AMSU brightness temperatures for channel 8 (left), 9 (center), and 10 (right). Scanning is restricted to only one scan direction, pixels 1 to 15 (top) or pixels 16 to 30 (bottom). Median, mean and standard deviation are shown in 10° bins and for the whole distribution.

- AMSU measurements need substantial bias corrections when they are assimilated in NWP models or used in climate studies. RO data are essentially bias-free and are treated as such in the operational variational bias correction scheme e.g. at ECMWF. Collocated RO observations provide an unique opportunity to validate and calibrate the measurements independent of such variational assimilation schemes. The detected biases for AMSU should then also be compared to the bias corrections generated by the ECMWF operational bias correction scheme.

- The remarkably good agreement between AMSU and ECMWF data poses an open question which should be investigated further.

- Using RO for monitoring and calibrating nadir sounders is not limited to AMSU—future work should address the other nadir temperature sounders on board of Metop as well (IASI and HIRS). A further interesting future prospect could be to use collocated radiosonde data as an additional source of information.

- Continuous collocating of RO and nadir sounders could allow long-term monitoring and calibrating of these instruments in the future. This could allow to deliver Fundamental Climate Data Record (FCDR) products as defined by GCOS also with these nadir sounders.

Acknowledgments

This study was conducted at the Danish Meteorological Institute (DMI), Copenhagen as part of EUMETSAT's GRAS-SAF visiting scientist program. I wish to thank Kent Bækgaard Lauritsen, Hans Gleisner, Kjartan Kinch, Stig Syndergaard, Hallgeir Wilhelmsen, Johannes Nielsen, and Frans Rubek for many fruitful discussions and their great hospitality at the DMI. I also thank Axel von Engeln, Christian Marquardt and Jörg Ackermann from EUMETSAT, Darmstadt for providing data and for helpful discussions.

Acronyms

AMSU Advanced Microwave Sounding Unit. 1–20

DMI Danish Meteorological Institute. 24

ECMWF European Centre for Medium-Range Weather Forecasts. 2, 7, 8, 12–16, 20

EPS EUMETSAT Polar System. 3, 4

EUMETSAT European Organization for the Exploitation of Meteorological Satellites. 3–5, 7, 8, 20

FCDR Fundamental Climate Data Record (As defined by GCOS). 20

GCOS Global Observing System for Climate. 3, 20

GNSS Global Navigation Satellite System. 3, 20

GPS Global Positioning System. 2, 4, 9, 10, 18

GRAS GNSS Receiver for Atmospheric Sounding. 2–5, 7, 9, 18, 21

GRAS SAF GRAS Satellite Application Facility. 7

HIRS High resolution Infrared Radiation Sounder. 3, 4, 20

IASI Infrared Atmospheric Sounding Interferometer. 3, 4, 20

IFOV Instantaneous Field of View. 6

LEO Low Earth Orbit. 4

LST Local Solar Time. 4

MetOp Meteorological Operational satellite series. 2–5, 8, 9, 18, 20

MSIS Mass Spectrometer and Incoherent Scatter Radar (atmospheric model). 2, 7, 12, 14, 15

MSU Microwave Sounding Unit. 2, 5, 7, 20

NOAA National Oceanic and Atmospheric Administration. 2, 3, 5, 21

NWP Numerical Weather Prediction. 3, 10, 11, 20

POES Polar Operational Environmental Satellite. 5

RO Radio Occultation. 1–5, 7–21

ROPP RO Processing Package. 7

RTTOV Radiative Transfer for TOVS. 8, 15

TIROS Television Infrared Observation Satellite. 5

TOVS Tiros Operational Vertical Sounder (Suite of vertical sounding instruments, flying on NOAA polar orbiting satellites). 8, 21

References

ATOVS Level 1b Product Guide (2010). v3. Ref.: EUM/OPS-EPS/MAN/04/0030. EUMETSAT. URL: http://www.eumetsat.int/Home/Main/DataProducts/Resources/index.htm?l=en (cit. on p. 8).

Cardinali, C. (2009). *Forecast sensitivity to observation (FSO) as a diagnostic tool*. Tech. rep. 599. ECMWF (cit. on p. 15).

Christy, J., D. Seidel, and S. Sherwood (2006). "What kinds of atmospheric temperature variations can the current observing systems measure and what are their strengths and limitations, both spatially and temporally?" In: ed. by T. Karl, S. Hassol, C. Miller, and W. Murray. Washington, DC: U.S. Climate Change Science Program/Subcommittee on Global Change Research. Chap. 2, pp. 29–46 (cit. on p. 4).

Engeln, A. von, C. Accadia, J. Ackermann, C. Marquardt, Y. Andres, D. Lazaro, and K. Klaes (2011). "Potentials for radio occultation applications during inter-satellite calibration periods". In: *Adv. Space Res.* 47.10, pp. 1731–1742. DOI: 10.1016/j.asr.2010.05.001 (cit. on p. 5).

GCOS (2010). *Implementation plan for the Global Observing System for Climate in support of the UNFCCC, (2010 Update)*. WMO-TD/No. 1523 GCOS-138 (GOOS-184, GTOS-76). WMO (cit. on p. 4).

Gorbunov, M. E., K. B. Lauritsen, A. Rhodin, M. Tomassini, and L. Kornblueh (2006). "Radio holographic filtering, error estimation, and quality control of radio occultation data". In: *J. Geophys. Res.* 111, D10105. DOI: 10.1029/2005JD006427 (cit. on p. 9).

Ho, S.-P., M. Goldberg, Y. H. Kuo, C. Z. Zou, and W. Schreiner (2009a). "Calibration of temperature in the lower stratosphere from microwave measurements using COSMIC Radio Occultation data: preliminary results". In: *Terr. Atmos. Ocean. Sci.* 20.1, pp. 87–100. DOI: 10.3319/TAO.2007.12.06.01(F3C) (cit. on p. 5).

Ho, S.-P. et al. (2009b). "Estimating the uncertainty of using GPS radio occultation data for climate monitoring: Intercomparison of CHAMP refractivity climate records from 2002 to 2006 from different data centers". In: *J. Geophys. Res.* 114, D23107. DOI: 10.1029/2009JD011969 (cit. on p. 12).

Karl, T. R., S. J. Hassol, C. D. Miller, and W. L. Murray, eds. (2006). *Temperature trends in the lower atmosphere: Steps for understanding and reconciling differences*. Washington, DC: U.S. Climate Change Science Program/Subcommittee on Global Change Research (cit. on p. 4).

Klaes, K. D., M. Cohen, Y. Buhler, P. Schlüssel, R. Munro, J.-P. Luntama, A. v. Engeln, E. O. Clérigh, H. Bonekamp, J. Ackermann, and J. Schmetz (2007). "An Introduction to the EUMETSAT Polar system". In: *Bull. Amer. Meteor. Soc.* 88.7, pp. 1085–1096. DOI: 10.1175/BAMS-88-7-1085 (cit. on p. 5).

Leroy, S., J. Dykema, and J. Anderson (2006).
"Climate Benchmarking Using GNSS Occultation".
In: *Atmosphere and Climate: Studies by Occultation Methods*.
Ed. by U. Foelsche, G. Kirchengast, and A. Steiner. Springer Berlin Heidelberg,
pp. 287–301. ISBN: 978-3-540-34121-5. DOI: 10.1007/3-540-34121-8_24
(cit. on p. 5).

Leroy, S., J. G. Anderson, and G. Ohring (2008). "Climate signal detection times and constraints on climate benchmark accuracy requirements".
In: *J. Climate* 21.4, pp. 841–846. DOI: 10.1175/2007JCLI1946.1 (cit. on p. 5).

Luntama, J., G. Kirchengast, M. Borsche, U. Foelsche, A. Steiner, S. Healy,
A. von Engeln, E. O'Clérigh, and C. Marquardt (2008).
"Prospects of the EPS GRAS Mission For Operational Atmospheric Applications".
In: *Bull. Amer. Meteor. Soc.* 89.12, pp. 1863–1875.
DOI: doi:10.1175/2008BAMS2399.1 (cit. on p. 7).

Offiler, D., H. Lewis, and I. Culverwell (2011).
Radio Occultation Processing Package (ROPP): An Overview. Tech. rep.
Ref.: SAF/GRAS/METO/UG/ROPP/001.
EUMETSAT Satellite Application Facility on GRAS Meteorology.
URL: http://www.grassaf.org (cit. on p. 8).

Santer, B. D., P. W. Thorne, L. Haimberger, K. E. Taylor, T. M. L. Wigley,
J. R. Lanzante, S. Solomon, M. Free, P. J. Gleckler, P. D. Jones, T. R. Karl,
S. A. Klein, C. Mears, D. Nychka, G. A. Schmidt, S. C. Sherwood, and F. J. Wentz (2008). "Consistency of modelled and observed temperature trends in the tropical troposphere". In: *Int. J. Climatol.* 28.13, pp. 1703–1722. DOI: 10.1002/joc.1756
(cit. on p. 4).

Santerre, R. (1989). *GPS Satellite Sky Distribution: Impact on the Propagation of Some Important Errors in Precise Relative Positioning*. Ph.D dissertation.
Fredericton, New Brunswick, Canada: Department of Surveying Engineering,
University of New Brunswick (cit. on pp. 11, 12).

Saunders, R. (2011a). *RTTOV-10 Science and Validation Report*.
NWP SAF NWPSAF-MO-TV-023. EUMETSAT (cit. on p. 10).

– (2011b). *RTTOV-10 Users Guide*. NWP SAF NWPSAF-MO-UD-023. EUMETSAT
(cit. on p. 10).

Scherllin-Pirscher, B., A. Steiner, G. Kirchengast, Y.-H. Kuo, and U. Foelsche (2011).
"Empirical analysis and modeling of errors of atmospheric profiles from GPS radio occultation". In: *Atmos. Meas. Tech.* 9, pp. 1875–1890.
DOI: 10.5194/amt-4-1875-2011 (cit. on p. 12).

Spencer, R. W. and J. R. Christy (1990).
"Precise Monitoring of Global Temperature Trends from Satellites".
In: *Science* 247.4950, pp. 1558–1562. DOI: 10.1126/science.247.4950.1558
(cit. on p. 7).

Steiner, A., G. Kirchengast, B. Lackner, B. Pirscher, M. Borsche, and U. Foelsche (2009). "Atmospheric temperature change detection with GPS radio occultation

1995 to 2008". In: *Geophys. Res. Lett.* 36, L18702. DOI: 10.1029/2009GL039777 (cit. on p. 5).

Thorne, P. W., D. E. Parker, J. R. Christy, and C. A. Mears (2005). "Uncertainties in climate trends: Lessons from upper-air temperature records". In: *B. Am. Meteorol. Soc.* 86, pp. 1437–1442. DOI: 10.1175/BAMS-86-10-1437 (cit. on p. 4).

Thorne, P. W., J. R. Lanzante, T. C. Peterson, D. J. Seidel, and K. P. Shine (2011). "Tropospheric temperature trends: history of an ongoing controversy". In: *Wiley Interdisciplinary Reviews: Climate Change* 2.1, pp. 66–88. DOI: 10.1002/wcc.80 (cit. on p. 4).

Trenberth, K. E., P. Jones, P. Ambenje, D. Bojariu, D. Easterling, A. Klein Tank, D. Parker, F. Rahimzadeh, J. Renwick, M. Rusticucci, B. Soden, and P. Zhai (2007). "Observations: Surface and Atmospheric Climate Change". In: *Climate Change 2007: The Physical Science Basis. Contribution of Working Group I to the Fourth Assessment Report of the Intergovernmental Panel on Climate Change*. Cambridge, UK and New York, NY, USA: Cambridge University Press. Chap. 3, pp. 237–336. URL: http://www.ipcc.ch/pdf/assessment-report/ar4/wg1/ar4-wg1-chapter3.pdf (cit. on p. 4).